In Vitro Reconstitution of Argonaute poly(ADP-ribosyl)ation and Its Impact on microRNA Activity

by
Ryan Weltzer

A thesis submitted to Johns Hopkins University in conformity with
the requirements for the degree of Master of Science

Baltimore, Maryland
November, 2013

Abstract

MicroRNA-mediated gene regulation is an important component of cell biology, involved in nearly all cellular processes. MicroRNAs are ~22 nucleotide non-coding RNAs that recognize complimentary mRNA targets and prevent them from being translated. To achieve this, the microRNA (miRNA) must be accompanied by one or more proteins known collectively as the RNA-induced silencing complex (RISC). The central component of the RISC is one of four Argonaute proteins. One of these proteins, Ago2, has endonuclease activity. Guided by a miRNA, Ago2 can directly cleave the mRNA target without assistance from any other RISC members. MiRNA repression is reduced upon stress when all Argonaute members, including Ago2, are modified by poly(ADP-ribose). Similar reduction in microRNA repression occurs upon knockdown of poly(ADP-ribose) degrading enzyme PARG or, conversely, by overexpression of specific poly(ADP-ribose) polymerases including PARP-12 and PARP-13. Moreover, Ago2 has been shown to be associated with PARP-5a, PARP-12 and PARP-13 by co-immunoprecipitation and co-localization at stress granules.

The aim of this project is to use recombinant proteins to ADP-ribosylate Ago2 *in vitro* to determine whether and how this modification affects Ago2-mediated RNA activity and if the modification can be reversed by PARG or another poly(ADP-ribose) hydrolase, ARH3. This thesis will describe the purification of ARH3 and the catalyctic domain of PARP-12 from *E. coli*. ARH3 is demonstrated to be an active glycohdrolase and PARP-12^{cat} is demonstrated to be a mono(ADP-ribose) tranferase. Our results suggest that Ago2 can be mono(ADP-ribosyl)ated by PARP-12^{cat} and may be poly(ADP-

ribosyl)ated by PARP-5a *in vitro*. Finally, an Ago2 cleavage assay has been recapitulated and optimized.

The work in this thesis project has established the necessary tools to test the hypothesis that mono(ADP-ribosyl)ation or poly(ADP-ribosyl)ation will repress Ago2 activity and whether its activity can be recovered with PARG or ARH3. Other future experiments may elucidate the role of PARP-13.

Thesis Advisor:

Dr. Anthony K.L. Leung

Thesis Reader:

Dr. Jürgen Bosch

Acknowlegements

Great thanks are due to Dr. Anthony K.L. Leung, who has been a patient and optimistic mentor. He has instilled in me an appreciation for rigorous scientific examination both in and out of the lab. Leung lab members Dr. Yoshinari Ando, Casey Daniels and Temitope Gafaar have been helpful, engaged and supportive of my project.

Dr. Jürgen Bosch, my thesis reader, gave me the experience I needed to join this degree program by allowing me to work in his lab for the two years prior. Without the knowledge of protein structural biology I learned in his lab, this project would not have been feasible.

Finally, I would like to thank my wife, Adelaide-Ulricke Paulina Hain, my parents, Darlene and Ernest, and my brother, Trevor, for their support and enthusiasm.

Table of Contents

List of Tables

List of Figures

List of Abbreviations

ARH3	poly(ADP-ribose) hydrolase 3
ARTD	ADP-ribosyltranferase
BME	β-mercaptoethanol
DTT	dithiothreitol
FPLC	fast protein liquid chromatography
GST	glutathione S-transferase
IPTG	isopropyl β-D-1-thiogalactopyranoside
kDa	kilodalton
LB	Luria broth
MAR	mono(ADP-ribose)
MART	mono(ADP-ribose) transferase
NAD+	nicotinamide adenine dinucleotide
PAR	poly(ADP-ribose)
PARG	poly(ADP-ribose) glycohydrolase
PARP	poly(ADP-ribose) polymerase
RISC	RNA-induced silencing complex
SDS-PAGE	sodium dodecyl sulfate-polyacrylamide gel electrophoresis
TRF1	telomeric repeat binding factor-1
UTR	untranslated region

Chapter 1

Background & Introduction

1.1 MicroRNA and Argonaute

MicroRNAs are short, non-coding RNAs involved in post-transcriptional gene regulation. After processing, a mature microRNA (miRNA) is 18-25 nucleotides long and single-stranded. It joins a complement of proteins, the RNA-induced silencing complex (RISC). In humans, the RISC-mediated miRNA pairs imperfectly to the 3' UTR of transcribed mRNA, inhibiting translation or initiating cleavage. Because the pairing is imperfect, each miRNA can bind multiple mRNA targets, allowing it to regulate multiple genes. Over 1500 miRNAs have been identified in humans (miRBase) (Griffiths-Jones et al, 2006), each one with the potential to regulate multiple genes, and is involved in regulating nearly all cellular activities (Liu et al, 2004; Meister et al, 2004).

MiRNAs may be transcribed from unique genes or from introns of protein coding genes by RNA polymerase II. These transcripts form a double-stranded hairpin known as a primary miRNA (pri-miRNA), stabilized by a double-stranded RNA binding protein. Still in the nucleus, the enzyme Drosha processes the pri-miRNA into a relatively shorter double-stranded hairpin structure of about 70 nucleotides, termed pre-miRNA. The pre-miRNA may also be more directly formed as a spliced-out intron of a protein-coding mRNA. This pre-miRNA from either source is then exported from the nucleus. In the cytosol, the pre-miRNA joins one of four Argonaute proteins, forming the basis of the RISC. Its hairpin structure is cleaved by the RNase Dicer yielding a miRNA/miRNA* duplex. The complementary miRNA* strand is left behind and either degraded or can

become its own miRNA. The main "guide strand" remains with Argonaute. Now approximately 20bp and single-stranded, the guide strand is free to base-pair with mRNA, bringing Argonaute and various other RISC proteins along (Krol et al, 2010). Although the first few miRNAs discovered reduced protein expression by inhibiting mRNA translation, it now appears that at least 84% of the time, miRNA targets are directed for degradation (Guo et al, 2010).

Of the four Argonautes, only Argonaute2 (Ago2) has the ability to cleave target mRNA directly. Ago2 has endonuclease activity conferred by its PIWI domain toward the target's phosphodiester bonds (Rivas et al, 2005). PIWI is found in a wide variety of RNA-interacting proteins. It contains a positively charged channel for RNA sugar-phosphate binding and an RNase H-like fold for target cleavage (Parker et al, 2004). Ago2 and the other members of the Argonaute family mediate RNAi using both small interfering RNA (siRNA) and miRNA. Upon binding, Ago2 bends a miRNA, creating several functional domains within the miRNA. The seed sequence, nucleotides 2-8, is most important for mRNA target recognition. The 3' complementary region adds further recognition (Wee et al, 2012).

1.2 Poly(ADP-ribosyl)ation and PARP-5a

ADP-ribosylation is a post-translational protein modification in which one or more ADP-ribose groups are covalently attached to an amino acid substrate (Fig. 1). Enzymes that catalyze this modification are termed poly(ADP-ribose) polymerases (PARPs), mono(ADP-ribose) tranferases (MARTs) or, more generally, ADP-ribosyltranferases (ARTD) (reviewed in Vyas et al, 2013). PARPs hydrolyze NAD^+ into

an ADP-ribose which is attached to the substrate with the nicotinamide left over. The ADP-ribose monomer may then be polymerized into linear or branching chains from 2-200 subunits long (Bürkle, 2005). This modification is reversible by several glycohydrolases, described later.

The founding member of the PARP family is PARP-1, well-characterized for its role in DNA damage recognition. In humans, seventeen PARPs have been identified based on homology to the PARP-1 catalytic domain. They have been divided into four subcategories based on domain structure: DNA-dependent, tankyrases, CCCH RNA binding and macroPARPs. Among these, PARPs 1-5a&b have been identified as able to build poly(ADP-ribose) chains. The remaining PARPs have identified or predicted mono(ADP-ribose) activity, and two are catalytically inactive (Gibson & Kraus, 2012).

PARP-5a, also called Tankyrase1, was first identified as a telomere-associated protein with the ability to poly(ADP-ribosyl)ate (PARylate) telomeric repeat binding factor-1 (TRF1) (Smith et al, 1998). In addition to its characteristic C-terminal PARP domain, it contains 24 ankyrin repeats, a motif which mediates protein-protein interactions. PARP-5a has since been shown to localize to mitotic spindle poles, endocytic vesicles (Hsiao & Smith, 2008) and more recently to stress granules (Leung et al, 2011). PARP-5a interacts with substrate partners through its ankyrin repeats, which recognize an eight amino acid motif, RSPPDGQS (Guettler et al, 2011). This sequence, with some variability, has been identified in many potential substrates and validated in such proteins as TRF1, tumor suppressor AXIN1/2, mitotic spindle regulator NUMA1, apoptosis regulator MCL1 (Guettler et al, 2011). The catalytic PARP domain of PARP-5a

is similar to other PARPs and centers around a catalytic triad of histidine, tyrosine and glutamate (Lehtiö et al, 2008).

PARP name	ARTD number	Other name	Subcategory	Transferase activity	Localization
PARP-1	1		DNA-dependent	PAR	Nuclear
PARP-2	2		DNA-dependent	PAR	Nuclear
PARP-3	3		DNA-dependent	PAR (pred)	Nuclear
PARP-4	4	vPARP	unclassified	PAR	Nuclear
PARP-5a	5	Tankyrase 1	Tankyrase	PAR	Nuclear & cytosolic
PARP-5b	6	Tankyrase 2	Tankyrase	PAR	Nuclear & cytosolic
PARP-6	17		unclassified	MAR (pred)	
PARP-7	14	tiPARP	CCCH RNA-binding	MAR (pred)	
PARP-8	16		unclassified	MAR (pred)	
PARP-9	9	BAL1	macroPARP	inactive	
PARP-10	10		unclassified	MAR	Nuclear & cytosolic
PARP-11	11		unclassified	MAR (pred)	
PARP-12	12		CCCH RNA-binding	MAR	Cytosolic, stress granule
PARP-13	13	ZAP	CCCH RNA-binding	inactive	Cytosolic, stress granule
PARP-14	8	BAL2	macroPARP	MAR	Cytosolic, stress granule
PARP-15	7	BAL3	macroPARP	MAR (pred)	Cytosolic, stress granule
PARP-16	15		unclassified	MAR (pred)	

(Gibson & Kraus, 2012; Kleine et al, 2008; Vyas et al, 2013)

Table 1: Overview of PARP family proteins
PARPs were identified based on their homology to the catalytic domain of PARP-1 and subdivided based on other structural features. If a member's activity has not been shown, it is designated as predicted (pred).

1.3 Mono(ADP-ribosyl)ation, PARP-12 and PARP-13

Less is known about PARPs 6-16, which make up the CCCH and macroPARP subgroups, all of which are predicted to have mono(ADP-ribosyl)ating activity, though PARP-9 and PARP-13 are catalytically inactive (Kleine et al, 2008). Unlike PARPs, which use a glutamate in their catalytic triad, MARTs lack this glutamate and it is proposed that they make use of a glutamate on the substrate to complete the attachment (Kleine et al, 2008). Therefore, once the site is modified, the catalytic glutamate is no longer available to assist transfer of any further ADP-ribose groups to lengthen the chain.

In humans, MAR is involved in transcription regulation through modification of histones and histone deacetylases (Feijs et al, 2013). Among the PARPs which localize to stress granules are PARPs 12 and 13. Overexpression of PARP-12 or PARP-13 results in a decrease of miRNA-mediated translation repression activity (Leung et al, 2011). Both also have demonstrated anti-viral activity, although the mechanism by which they do so is unknown. PARP-12 is expressed in two isoforms, one with and one without its PARP domain, but only the full-length product is able to inhibit viral replication(Atasheva et al, 2012). PARP-13 also exists in two isoforms and requires its PARP domain to inhibit alphavirus replication by inducing innate immune responses (Kerns et al, 2008). It may also have an antiviral role without its PARP domain, as it has been shown to be selectively induced by 5'-triphosphate modified RNA (Hayakawa et al, 2010). Furthermore, the catalytic domain of PARP-13 may not have any ADP-ribose transferase activity at all (Leung et al, 2011). Unlike other recombinantly expressed catalytic domains, PARP-13^{cat} does not auto ADP-ribosylate (Kleine et al, 2008).

1.4 PARPs and Ago2 colocalize at stress granules

Argonaute proteins are modified by PAR under normal conditions. Upon stress, PARylation of Ago2 increases, leading to a decrease in its miRNA-mediated repression. This modification only occurs when the mRNA-binding PIWI domain is present, suggesting that the modification happens on this domain or that mRNA binding is necessary for PAR modification. During stress, Ago2 localizes to stress granules in the cytoplasm along with two isoforms of poly(ADP-ribose) glycohydrolase, PARG99, PARG102 and five PARPs: 5a, 12, 13, 14 and 15. Overexpression of PARP-12, 13.1 and 13.2 led to a decrease in miRNA activity. The mechanism for PARP-13-mediated miRNA repression is unclear because PARP-13.1 has not been shown to have an active PARP domain and PARP-13.2 lacks this domain altogether. These PARPs themselves are ADP-ribosylated, creating a complex network of cross-regulation (Leung et al, 2011). Ago2 IP extract, mixed with cell extracts overexpressing PARP combinations indicate that 5a/12, 5a/13.2 and 12/13.2 resulted PARylation greater than that of PARP-5a alone (unpublished).

1.5 Reversal of PARylation

PARylation is reversed by several identified glycohydrolases, poly(ADP-ribose) glycohydrolase (PARG) and poly(ADP-ribose) hydrolase 3 (ARH3). The competition between PARPs to build PAR chains and the hydrolases to degrade them provides a mechanism for fine tuning of PAR regulation.

PARG cleaves ribose-ribose bonds between PAR subunits (Lin et al, 1997), shown in Figure 1, but cannot cleave the terminal monomer from its protein substrate

(Slade et al, 2011). PARG mRNA is alternatively spliced to produce at up to four isoforms, all of which share the catalytic domain. The full length product, hPARG111 (named for its molecular weight) localizes to the nucleus, while hPARG102 and hPARG97 are cytoplasmic (Meyer-Ficca et al, 2004). A fourth isoform, hPARG60 was reported to be found at the mitochondria (Meyer et al, 2007). The mRNA for hPARG60, was found to be spliced into an even shorter version, hPARG55, which is present at the mitochondria but not active there (Niere et al, 2012).

ARH3 is a distinct glycohydrolase, sharing 19% sequence identity to PARG in its catalytic domain. Its crystal structure (Mueller-Dieckmann et al, 2006) reveals that its catalytic fold is unique from that of PARG (Kim et al, 2012). It is specific for PAR but not MAR, but with only approximately 10% of the efficiency of PARG *in vitro* (Oka et al, 2005). ARH3 is present in the cytosol, nucleus and mitochondria. Its N-terminus carries a mitochondrial localization signal, and it is active in the mitochondrial matrix (Niere et al, 2012).

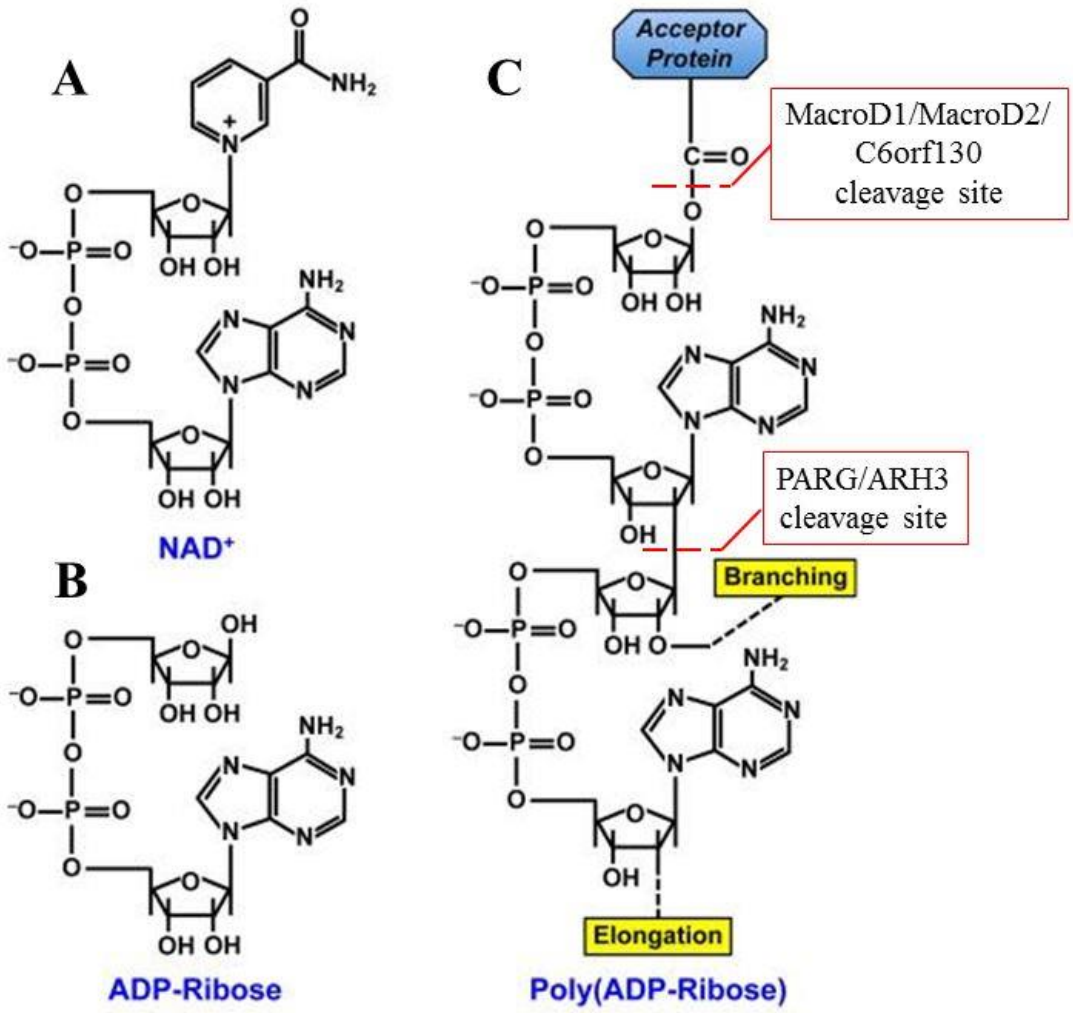

Adapted from (Luo & Kraus, 2012)

Figure 1: Diagram of poly(ADP-ribose) synthesis and degradation
Members of the PARP family cleave the nicotinamide moiety from substrate NAD^+ (A), resulting in ADP-ribose (B). A MART or PARP can attach it to an amino acid substrate, but only PARPs can elongate the chain (C). PAR chains can be linear or branched, depending on catalytic ability of the PARP. The PAR 2-mer shown above is a linear chain, but a branching chain could be built from the site indicated. PAR is degraded by glycohydrolases PARG and ARH3 between ribose groups.

1.6 Reversal of MARylation

Although it was long known that mono(ADP-ribosyl)ation (MARylation) could be reversed, it was only recently that several proteins with the ability to remove MAR modifications were discovered (hydrolysis site shown in Fig. 1). The first, C6orf130, was discovered in the context of neurodegeneration. When its gene is mutated with a premature stop codon, a truncated protein product results in a phenotype characterized by seizures and severe neurodegeneration. This defect is linked with a loss of the ability to cleave MAR (Sharifi et al, 2013). Two other proteins, MacroD1 and MacroD2, were subsequently identified. All three proteins carry a macrodomain, a domain known to bind MAR and PAR. Each is able to hydrolyze MAR from auto-modified PARP-10, a mono(ADP-ribose) transferase (Rosenthal et al, 2013). C6orf130 has limited ability to hydrolyze PAR chains (Sharifi et al, 2013), whereas MacroD1 and MacroD2 cannot (Rosenthal et al, 2013). MacroD2 was further characterized as having the ability to remove the terminal monomer from PARP-1 after the longer PAR chain was treated with PARG (Rosenthal et al, 2013). The presence of MacroD2 can inhibit the ability of PARP-1 to form PAR chains (Jankevicius et al, 2013), adding another layer of regulation to the ADP-ribose modification system. Although all three proteins have similar activity *in vitro*, MacroD1 localizes to the mitochondria, and the neurological role of C6orf130 suggests their environments and substrates may differ (Feijs et al, 2013).

1.7 Conclusion

Previous work strongly suggests a model in which, under stress conditions, Ago2 is sequestered to stress granules where it is PARylated. While PARylated, Ago2 would

be unable to mediate miRNA induced silencing, allowing potential mRNA targets to be translated in response to the stress situation. There are several levels of fine-tuning within this model. Ago2 could be MARylated or PARylated, perhaps resulting in different levels of modification, or MARylation could promote faster PARylation by getting the chain started. This would depend on the presence of MARTs like PARP-12 or PARPs like PARP-5a. PARP-5a itself may need a boost from PARP-12 or PARP-13.2 to PARylate Ago2, discussed in section 3.5. Furthermore, all of these PARPs can be MARylated and PARylated by themselves or other PARPs, likely affecting in some way their ability to modify Ago2. Finally, the presence or absence of PARG in its various isoforms or ARH3 gives yet another mechanism for regulation. The potential network of cross-modification and reversal is complex. The aim of this project is to isolate components in an *in vitro* setting to verify the hypotheses generated by previous work. Then, step by step, the network can be rebuilt, examining the effect of each component and its effect on the overall system. Here, the purification and activity of PARP-12 and ARH3 are described. This thesis will outline the progress toward MARylating and PARylating Ago2. Finally, a miRNA-guided Ago2 cleavage assay is reconstituted. This work builds the necessary components for an *in vitro* reconstruction of events occurring at stress granules and more specifically, to determine whether ADP-ribosylation hinders Ago2-mediated RNA silencing.

Chapter 2

Materials & Methods

2.1 Protein Expression and Purification

2.1.1 ARH3 Expression and Purification

Expression and purification of human protein ADP-ribosylhydrolase (ARH3) in *E. coli* followed published methods (Kernstock et al, 2006). The expression plasmid was obtained from Joel Moss (Oka et al, 2005). The vector, pGEX-2T contains a glutathione S-transferase (GST) tag and a thrombin cleavage site, followed by the coding sequence of ARH3 and an Ampicillin resistance gene for selection. ARH3 is 39kDa (Oka et al, 2005) and GST is 26kDa, resulting in a fusion product of 65kDa. Approximately 100ng plasmid was transformed into 50µL chemical-competent Rosetta 2(DE3) *E. coli*. Rosetta 2 cells have chloramphenicol resistance on a plasmid optimizing for expression of eukaryotic codons. After transformation, the cells were used to inoculate 5mL LB containing 50µg/mL ampicillin and 35µg/mL chloramphenicol. This starter culture was grown overnight at 37ºC, shaking at 200rpm. *E. coli* was pelleted by centrifugation and resuspended in 50mL LB with the same concentrations of antibiotics. Growth continued at 37ºC with shaking. When the culture was visibly turbid, the cells were again pelleted by centrifugation and resuspended in 1L LB with antibiotics and 50µL antifoam. As the culture grew, the optical density at a wavelength of 600nm was periodically measured by spectrophotometer. When OD_{600} reached 0.7, protein expression was induced with 0.5mM IPTG. The temperature was lowered to 20ºC and expression continued overnight.

All following purification steps were carried out at 4ºC or on ice unless specified. Cells were harvested by centrifugation at 4500rpm for 20 minutes and resuspended in 35mL lysis buffer containing 50mM Tris-HCl (pH 8.0), 150mM NaCl, 10mM $MgCl_2$, 0.1%v/v Triton X-100, 3mM BME, EDTA-free protease inhibitor cocktail (Roche) and 200 units DNase I (Roche). Cells were lysed by mechanical homogenization (Avestin EmulsiFlex-C5) and clarified by centrifugation at 18000rpm for 40 minutes. The supernatant was collected and incubated while rocking with 1mL glutathione agarose beads (Sigma) for 30 minutes. The supernatant/bead slurry was applied to an open gravity flow column. The flow-through was collected for later analysis. Beads in the column were washed with 10 column volumes of lysis buffer followed by 10 column volumes of the same buffer without Triton X-100. ARH3 was cleaved from GST on-column by addition of 10 units of thrombin (GE Healthcare) in 1mL wash buffer. The cleavage reaction was incubated at room temperature for 4 hours with occasional swirling. The buffer was collected, followed by 4x1mL washes to clear additional cleaved protein. Remaining protein was eluted with 20mM reduced glutathione, 50mM Tris-HCl (pH 8.0), 75mM NaCl, 10mM $MgCl_2$ and 3mM BME. Whole cells, insoluble fraction, column flow-through, wash, each of the five cleaved elutions and the uncleaved elution were analyzed on a 12% SDS-PAGE minigel with a size marker (PageRuler broad range prestained protein ladder). The gel was rinsed in water, stained with coomassie (SimplyBlue SafeStain), destained in water and scanned on the Odyssey (Fig. 2). The five 1mL cleaved fractions were pooled and concentrated to 500µL in a 10kDa-cutoff concentration tube. The concentrated sample was centrifuged at top speed in a tabletop centrifuge for 10 minutes to pellet any precipitated protein. Supernatant was loaded onto

a Superdex 200 size exclusion column (GE Healthcare) using the Äkta FPLC system. Protein was eluted by flowing buffer containing 50mM Tris-HCl (pH 8.0), 150mM NaCl, 10mM $MgCl_2$ and 3mM BME. Eluate was collected in 500µL fractions. Fractions corresponding to peaks measured at an absorbance of 280nm were analyzed by SDS-PAGE as described above (Fig. 2). A peak which eluted at an approximately expected size from the S200 column corresponded with the 39kDa band on SDS-PAGE. Fractions corresponding to this peak were pooled and concentrated in a 10kDa-cutoff filter. Size exclusion buffer with 10% glycerol was used to adjust the concentration to 5mg/mL as measured by NanoDrop. The sample was aliquoted, snap-frozen in liquid nitrogen and stored at -80ºC.

2.1.2 PARP-12^{cat} Expression and Purification

Expression and purification of the catalytic domain of human PARP-12 in *E. coli* roughly followed methods available online (http://www.thesgc.org/structures/details?pdbid=2PQF/). The plasmid construct was obtained from Torun Ekblad. The pNIC-bsa4 vector contains a 6xHistidine tag and Tobacco Etch Virus (TEV) cleavage site followed by the open reading frame, where PARP-12^{cat} is inserted. This encodes for a 219 amino acid, 25kDa protein. The construct was transformed into Rosetta 2 *E. coli* and a glycerol stock was made. The glycerol stock was poked to inoculate a starter 5mL overnight culture in LB with 50µg/mL kanamycin and 35µg/mL chloramphenicol. It was grown at 37ºC with shaking as described above. This culture was increased to 50mL LB with antibiotics until it was visibly turbid. It was then increased to 1L and later to 2L. When OD_{600} reached 0.7, the temperature was

lowered to 18ºC and allowed to equilibrate for 30 minutes before inducing with 0.5mM IPTG. Expression continued overnight.

Cells were harvested by centrifugation and resuspended in 40mL lysis buffer containing 50mM HEPES-NaOH (pH 8.0), 500mM NaCl, 10mM imidazole and 10% glycerol. The mixture was snap-frozen in liquid nitrogen and stored at -80ºC. To purify, the cells were thawed at room temperature then transferred to ice, after which all steps were carried out at 4ºC or on ice. DNase I and protease inhibitor cocktail was added before lysing by homogenization. Lysate was clarified by centrifugation and the supernatant was collected. The supernatant was loaded into a syringe and manually pumped over a 5mL nickel-charged HisTrap Crude FastFlow immobilized-metal affinity column (GE Healthcare). The column with bound protein was washed with 6 column volumes lysis buffer, followed by 2x5mL elutions with lysis buffer containing 300mM imidazole. Whole cells, insoluble and soluble fractions, nickel flow-through, wash and the elutions were run on 12% SDS-PAGE (Fig. 3A). The two elutions were combined and dialyzed overnight with 500mL dialysis buffer containing 30mM HEPES-NaOH (pH 7.5), 300mM NaCl and 10% glycerol. The elutions were extremely impure, so they were reloaded onto the nickel column, washed with 20 column volumes lysis buffer and eluted in 5mL steps of increasing imidazole concentration: 20mM, 50mM, 100mM, 150mM, 200mM, 250mM and 300mM. SDS-PAGE revealed PARP-12^{cat} to be primarily in the 100mM and 150mM steps, along with proteins of various other sizes (Fig. 3B). These fractions were combined and dialyzed overnight in dialysis buffer. The sample was further purified by ammonium sulfate precipitation. Solid ammonium sulfate was added while stirring on ice to 10% then spun at 10,000xg. The supernatant was collected and the

pellet was resuspended in 5mL lysis buffer. This was repeated with the supernatant to steps of 20%, 30%, 40% and 50%. All protein, including PARP-12^{cat} and impurities, precipitated at 40% and 50% ammonium sulfate (these two steps had similar coomassie gel profiles, seen in Fig. 3C). They were combined and dialyzed overnight into 500mL buffer A, containing 20mM HEPES-NaOH (pH 7.5), 10% glycerol and 2mM BME. After dialysis, the sample appeared cloudy, so it was spun at 500xg to pellet precipitated protein. The supernatant was collected and the pellet was saved for analysis. Clarified supernatant was hand-loaded by syringe on to a 5mL HiTrap Q FastFlow anion exchange column pre-equilibrated with buffer A. The column was washed with 2 volumes buffer A, then attached to the Äkta FPLC. Protein was eluted using a linear gradient of 0-1M NaCl over 10 column volumes and collected in 1mL fractions. The dialysis pellet, supernatant (HiTrap Q input), Q column flow-through and fractions corresponding to measured peaks were analyzed by SDS-PAGE (Fig. 3D). PARP-12^{cat} was observed in the Q wash and an early elution peak. These two fractions were kept separate. The wash was concentrated in a 10kDa-cutoff tube to 1.3mg/mL and the elution was concentrated to 0.7mg/mL. Each sample was aliquoted in separately labeled tubes, snap frozen in liquid nitrogen and stored at -80ºC.

2.1.3 PARP-5a Expression

Expression and purification of human PARP-5a (TNKS1) in insect cells was based on protocols provided by Susan Smith (Smith et al, 1998). Reagents, insect cells, equipment and instruction was provided by Yana Li in the Eukaryotic Cell Expression Facility at the Johns Hopkins School of Medicine. Baculovirus expanded once (P2) was

obtained from the Smith lab. This baculovirus plasmid (bacmid), contains the coding sequence for PARP-5a under a polyhedron promotor. A viral titer number was not available. 175µl of this stock was used to infect 500mL of *Spodoptera frugiperda* Sf9 cells at a density $2x10^6$/mL. The cells were incubated at 27°C, in a spinner flask to maintain the cells in suspension, for approximately 72 hours. At this point, roughly half the cells had died from viral infection, indicating successful viral propagation. The cells were spun down; the supernatant (media with virus) was collected and separated into 50mL aliquots. 25mL of this third passage (P3) was used to infect 200mL Sf9, this time optimizing for protein expression as opposed to virus propagation. Half of the culture was removed at 42 hours (at a density of $1.7x10^6$/mL) while the remainder was allowed to incubate until 70 hours ($2x10^6$/mL). Both were spun down immediately after harvesting. The supernatants were discarded; the pellets were flash-frozen in liquid nitrogen and stored at -80ºC. The samples were handled in parallel but kept separate during purification.

The pellets were thawed in cold lysis buffer containing 20mM Tris-HCl (pH 8.0), 500mM NaCl, and 5mM imidazole. Cells were lysed by sonication with three cycles of 30 seconds on, 30 seconds off. Lysate was clarified by centrifugation. The supernatant was syringe-pumped over a 5mL nickel-charged HisTrap FastFlow Crude column (GE). The column was washed with 10 volumes lysis buffer, then eluted with 2x5mL lysis buffer containing 300mM imidazole. Fractions were analyzed by SDS-PAGE, but no enrichment was observed at the expected size. A western blot was then performed with the same fractions, revealing an enriched band at the expected size, but also many other bands of various sizes.

Optimization of expression conditions was undertaken to produce more favorable results. 1L of Sf9 cells was split into four smaller spinner flasks. The four smaller cultures were infected with varying amounts of P3 virus: 2.5mL, 5mL, 10mL and 25mL. Half of each culture was harvested at 72 hours while the remainder was allowed to incubate until 96 hours, with the exception of the culture infected with 2.5mL P3, in which most cells were dead after 72 hours and were therefore harvested entirely at that time. This yielded 7 conditions, which were resuspended in lysis buffer before snap-freezing and stored at -80ºC until ready for purification. While thawing, protease inhibitors and DNase were added. Whole cells were analyzed by SDS-PAGE and western blot. No enrichment was visible in coomassie staining. The western blot, with PARP-5a-expressing HeLa cells and uninfected Sf9 cells used as controls, confirmed expression of PARP-5a, but did not provide better expression conditions. Cells were pooled, lysed by sonication and clarified by centrifugation. Supernate was affinity-purified by HisTrap Crude Fast Flow and analyzed by SDS-PAGE. The HisTrap elution showed proteins of all sizes. The elution was concentrated to 500µL in a 30kDa-cutoff tube and loaded onto an S200 size exclusion column using the Äkta FPLC. Concentration and S200 elution was done in buffer containing 20mM HEPES-NaOH (pH 8.0), 100mM KCl, 3mM MgCl2 and 2mM BME. Fractions containing proteins roughly corresponding to the expected size of PARP-5a were collected, concentrated with 10% glycerol to 5mg/mL, flash-frozen in aliquots and stored at -80ºC, despite being highly impure.

In the third expression attempt, P4 virus supplied by Titia deLange was used to directly infect 100mL of Sf9 cells. After lysing, the pellet was resuspended in buffer containing 1% NP-40 to aid in solubility.

The fourth expression used 10% fetal bovine serum during Sf9 growth which was washed away with media prior to lysis. Cobalt-charged TALON resin was substituted in the affinity capture step. Anion exchange chromatography using HiTrap Q FF was also tested. The insoluble fraction from this expression was resuspended in 8M urea to test the possibility of refolding insoluble PARP-5a. This was loaded on to nickel HisTrap FastFlow Crude, followed by washes of 7M, 6M, 5M, 4M and 1M urea in lysis buffer, then lysis buffer only.

Sf21 cells were tested in the fifth expression with de Lange lab P4 virus, but the yield was not improved. At this point, expression was put on hold until fresh bacmid could be produced. Numerous attempts to clone PARP-5a into a pre-bacmid pFastBac1 vector were unsuccessful.

2.2 Activity Assays

2.2.1 ARH3 Activity Assay

The ability of ARH3 to cleave PAR chains was tested on automodified PARP-1. The conditions for PARP-1 automodification and subsequent digestion with commercial $PARG^{cat}$ (Trevigen) were developed by Casey Daniels. Purified 6xHis-PARP-1 was provided by Casey. Several rounds of optimization generated consistency between replicates. First, 500ng (per reaction) PARP-1 was attached to 0.5µg MagneHis magnetic nickel beads (Promega) for 2 hours, rotating at 4ºC in attachment buffer containing 50mM Tris-HCl (pH 7.4), 1mM ADP-HPD (a PARG inhibitor), 1% Tween-20, 0.2mM DTT, 10% glycerol, 10mM $MgCl_2$ and protease inhibitors. With the protein attached, the beads were isolated against a magnet while the buffer was changed to automodification

buffer containing 20mM Tris-HCl (pH 7.5), 50mM NaCl, 50μM TCEP and 5mM $MgCl_2$. A mixture of ^{32}P-labeled and unlabeled NAD^+ was added to each condition, to be cleaved by PARP-1 and build into PAR chains for subsequent detection. The final NAD^+ concentration was 19μM, 1% of which was radioactive. To catalyze PARP-1 activity, blunt-end annealed DNA oligonucleotides were added to a working concentration of 1μM. The PARylation reaction proceeded for 30 minutes at 25ºC. An excess of unlabeled NAD^+ was added to promote the formation of the longest PAR chains possible, bringing the total concentration of NAD^+ above 2.5mM. After an additional hour at 25ºC, the beads/proteins were isolated by magnet, the buffer was removed and the beads were washed twice in 50μL wash buffer containing 50mM sodium phosphate (pH 7.4), 200mM NaCl, 5mM imidazole and 1% Tween-20. After washing, the buffer was replaced with digestion buffer containing 50mM potassium phosphate (pH 7.5), 50mM NaCl, 10mM $MgCl_2$, 1mM BME, 10% glycerol, 0.1% Triton X-100 and 1mM 3-AB (a PARP inhibitor). ARH3 at varying concentrations or 5ng $PARG^{cat}$ was added. After incubating for 2 hours at 25ºC, the buffer was removed and the beads were washed twice. Protein was eluted from the beads by boiling in SDS for 5 minutes at 95ºC in loading dye and analyzed by SDS-PAGE, followed by overnight autoradiography. This experiment was performed in duplicate. Controls included 500ng PARP-1 unattached input, attached unmodified PARP-1 carried through all washes and incubations, modified PARP-1 eluted immediately after modification, modified undigested PARP-1 carried through all steps and PARG digested (for comparison with ARH3).

2.2.2 PARP-12^{cat} Activity Assay

The ability for PARP-12^{cat} to auto-mono(ADP-ribosyl)ate was tested using a protocol adapted from PARP-1 automodification. One microgram per reaction 6xHis-tagged PARP-12^{cat} was attached to MagneHis magnetic nickel beads by incubating with rotation at 4ºC for 2 hours. The binding buffer was changed to automodification buffer and a mixture of labeled and unlabeled NAD^+ was added. After 30 minutes of incubation at 25ºC, the beads were washed twice and eluted by boiling in SDS loading dye. Samples were analyzed by 12% SDS-PAGE and autoradiograph. PARP-1 was included as a positive control for ADP-ribosylation and to compare its PAR activity with PARP-12's predicted mono(ADP-ribosyl)ation activity. Input and bead attachment controls were also included. PARP-12^{cat} species from both the anion exchange flow-through and elution, described in section 2.2.1, were tested for activity. The elution, which showed activity, was tested again in a 6µg batch, with 1µg removed, washed and heated with SDS loading dye every 5 minutes for 30 minutes.

PARP-12^{cat} was tested for the ability to mono(ADP-ribosyl)ate Ago2. Ago2, carrying endogenous insect cell RNA, was batch-bound to MagStrep beads overnight in binding buffer (buffers described in 2.2.1). The Ago2 was then split into six experimental conditions and mixed with PARP-12^{cat} in various amounts. In three conditions, Ago2 was constant at 1µg, with 62.5ng, 250ng or 1µg PARP-12^{cat}, resulting in molar ratios of 4:1, 1:1 and 1:4. In the next three conditions, PARP-12^{cat} was constant at 1µg with 250ng, 1µg or 2µg Ago2, resulting in molar ratios 8:1, 4:1 and 2:1. The buffer was changed to automodification buffer and NAD^+ was added to a concentration of 17.5µM, 1% ^{32}P-labeled. NAD^+ was added to all conditions except Ago2 and PARP-12^{cat} input lanes. This

was incubated for 30 minutes at 25ºC, washed twice, eluted in 15µL loading dye, boiled and analyzed by 12% SDS-PAGE.

2.2.3 PARP-5a Activity Assay

PARP-5a (Tankyrase1) with a 6xHistidine tag was purchased from Trevigen. It was tested for the ability to auto-PARylate and to modify substrates TRF1 and Argonaute2 (Ago2). Automodification was tested using the PARP-1 automodification protocol, minus the DNA. Using 100ng per condition, PARP-5a was tested for the ability to PARylate 500ng of known substrate TRF1 (Smith et al, 1998), 1µg Ago2 or 1µg BSA. Magnetic nickel beads were used for buffer changes and wash steps with PARP-5a only, with TRF1 and with BSA. MagStrep beads were used with PARP-5a with Ago2, as the MagStrep beads were observed to bind all protein indiscriminately. The concentration of NAD^+ was tested at 40µM (0.75% radioactive), 4µM (7.5% radioactive) and 0.3µM (100% radioactive). To further optimize modification of Ago2, several additions were tested: 536ng total RNA extracted from 293T cells provided by Yoshinari Ando or 200µL lysate from 293F cells over-expressing GFP-PARP-13.2 or GFP only, provided by Temitope Gafaar. Samples were analyzed by 8% SDS-PAGE and autoradiograph.

2.2.4 Argonaute2 cleavage assay

Two varieties of Argonaute2 (Ago2) were provided by the Leemor Joshua-Tor: with and without endogenous insect cell miRNA. Both were tested against two RNA targets: a perfect complement of bantam miRNA (5'-guaucaaaaucagcuuucacaaugaucucaacguucaau-3') and an imperfect target meant to serve

as a negative control (5'-guaucaaaauagcuuucaccccugauacucaacguucaau-3'). First, Ago2 with RNA was tested against these targets. Next, both species of Ago2 were incubated with bantam (5'-ccgguuuucgauuugguuugacu-3') (Thermo Scientific) before testing them against the targets. Targets were phosphorylated using T4 polynucleotide kinase (New England Biolabs) and ^{32}P labeled ATP (Perking Elmer). Bantam was phosphorylated with non-radioactive ATP. 2pmol Ago2 (200ng) was incubated with 2pmol bantam and 20units (1µL) SUPERase In RNase inhibitor (Ambion) and incubated at 26ºC for 90 minutes. This and all subsequent steps took place in buffer containing 40mM potassium acetate pH 7.4, 2mM $MgCl_2$ and 1mM DTT. Now loaded with bantam, 0.15pmol or 1.5pmol Ago2 was mixed with 0.15pmol target and 20 units RNase inhibitor at 30ºC for one hour. RNA was isolated by diluting the 10µL reaction with 190µL water, then mixing with 200µL buffer-saturated phenol pH 7.5 (Life Technologies). This was vortexed for one minute, then spun down at top speed on a tabletop centrifuge for 2 minutes to separate the phases. The upper aqueous phase was pipetted off, placed in a clean tube and mixed with 200µL of phenol:chloroform:isoamyl alcohol (25:24:1) pH 7.9 (Sigma). This was vortexed and spun as before. The aqueous layer was pipetted to a clean tube. RNA was precipitated by adding 20µL 3M sodium acetate pH 5.5, 1µL linear acrylamide, 600µL absolute ethanol and incubating at -80ºC for 15 minutes. This was spun at top speed at 4ºC for 30 minutes. The supernatant was discarded. The pellet was washed in cold 70% ethanol, spun for 10 more minutes at 4ºC and the supernatant was again discarded. The pellet was allowed to dry in a fume hood for several hours at room temperature. When dried, the pellet was resuspended in RNA loading buffer (Ambion), heated for 2 minutes at 95ºC and cooled on ice. Samples were loaded onto a denaturing

self-poured 12% ureagel (gel components from Sequagel) and electrophoresed for approximately 2.5 hours at a constant power of 35W. A 10 base-pair DNA ladder (Invitrogen) and a 22 nucleotide RNA (provided by Yoshinari Ando), both phosphorylated with ^{32}P ATP as described above, were run on the gel for size comparison. The gel was then exposed to autoradiography overnight. The autoradiograph was scanned on the phosphoimager (FujiFilm).

Material	Contributor
ARH3 expression plasmid	Joel Moss
PARP-12^{cat} expression plasmid	Torun Ekblad
Ago2 protein	Leemor Joshua-Tor
TRF1 protein	Leemor Joshua-Tor
PARP-5a expression baculovirus	Susan Smith, Titia de Lange
Äkta FPLC	Paul Miller

Table 2: Materials shared by collaborator labs

Chapter 3

Results & Discussion

3.1 ARH3 glycohydrolase activity

Expression of active human ARH3 was achieved on the second attempt. Optimizing induction to 0.5mM IPTG reduced the amount of insoluble protein observed in a primary attempt. The second expression was also the first time thrombin was used to cleave off the GST tag. After on-column cleavage, size exclusion purification and concentration, the final yield was approximately 1µg. Uncleaved GST fusion ARH3 was tested along with cleaved ARH3 in the first assay. While uncleaved protein did not appear to have the same level of activity as cleaved protein, the controls were not consistent between the duplicates. In subsequent assays, controls were optimized, but uncleaved protein was not tested further because of the low yield and concentration. Figure 4 shows the results of varying amounts of ARH3 cleaving PAR chains on automodified PARP-1. In the coomassie stain, PARP-1 unmodified input and bead attachment control lanes show that in addition to full length protein, indicated at 113kDa, there are many fragments extending down to 50kDa. During automodification, PAR chains are built on these fragments, in addition to the full-length protein, enhancing the smearing effect visible in the autoradiograph (Fig. 4, right). In the coomassie stain, PARP-1 disappears because of the variable size PAR chains, but appears as a smear on the autoradiograph. After treatment with $PARG^{cat}$, the chains are cleaved down to the terminal ADP-ribose moiety; distinct bands reappear and correspond with autoradiograph bands. When PARylated PARP-1 was mixed with 0.5µg ARH3, the smear decreases

somewhat. With 5µg ARH3, the autoradiograph smear is replaced by distinct bands, which also reappear on the coomassie stain, similar to the profile observed with $PARG^{cat}$ treatment. Unlike $PARG^{cat}$, 5µg ARH3 leaves a band of high molecular weight. Finally, with 50µg ARH3, the radioactive signal is totally ablated.

Discussion

Treatment of PARylated PARP-1 with increasing amounts of ARH3 demonstrates the ability of ARH3 to cleave PAR chains from PARP-1, though with significantly less efficiency than $PARG^{cat}$. 5µg of ARH3 is necessary to mimic the results of cleavage with 5ng $PARG^{cat}$, a thousand-fold increase by weight (though they are similar in size, so their molarity is similar). This is far less activity than previously reported (Oka et al, 2005). Even at this level of ARH3, there is some residual smearing, along with a high molecular weight band in the autoradiograph. Another difference is the intensity of the bands between 5µg ARH3 and $PARG^{cat}$. In the PARGcat condition, the bands are distinct and the signal is strong. The ARH3-generated bands not only show smearing in between, the bands themselves are weaker. Considering this, it seems possible that the activity of these two enzymes is not the same. Further, in the condition using 50µg ARH3, the absence of any signal could indicate that terminal ADP-ribose moieties have been removed, but this would need to be verified by further experiments, discussed below in section 4.1. This is an unexpected result, as it was previously reported that ARH3 is unable to reverse mono(ADP-ribosyl)ation (Oka et al, 2005).

3.2 PARP-12^{cat} mono(ADP-ribose) transferase activity

Although the first purification yielded enough protein for activity assays, more was needed for subsequent tests. Several steps from the initial purification appeared appropriate for optimization. The ammonium sulfate precipitation, in which all previously soluble proteins precipitated together, was dropped. Because a smaller band below the main 25kDa PARP-12^{cat} band appeared to enrich after anion exchange, further purifications included protease inhibitors not only during lysis and the affinity capture step, but also through to anion exchange, on the hypothesis that it may be a result of proteolytic cleavage. Because the theoretical isoelectric point (pI) of PARP-12^{cat}, calculated by Expasy ProtParam, is 6.86, the anion exchange buffer was increased in pH from 7.5 to 8.0, further from the pI, to promote tighter binding to the resin. This resulted in an elution peak from the anion exchange column at a similar salt concentration, but with a lower molecular weight. The only protein eluting at the correct size from this anion exchange step eluted with an abundance of higher-weight contaminants, and appeared smeared, which PARP-12^{cat} had not displayed before. The lower molecular weight protein was assayed for activity, but none was observed. Expression and purification was repeated, but the result was the same. The plasmid construct was then re-transformed into Rosetta 2 *E. coli* and expressed directly without freezing, in case the glycerol stock had degraded in quality after long-term deep freeze, but the result did not improve. Anion exchange fractions from that (fourth) purification were analyzed by western blot with an anti-his tag primary antibody. Early fractions showed distinct bands at 25kDa on the blot, but did not show activity when tested. Finally, a nickel-charged 5mL HiTrap Chelating HP column (GE) was substituted in the affinity capture step. This yielded the cleanest elution yet. This was further purified by anion exchange, with a pH

7.5 as in the original purification. As in the first purification, a protein of 25kDa eluted at low salt. This was concentrated to 1.5mg/ml, aliquoted, flash frozen and stored at -80ºC. Unfortunately, although this purification was the most promising yet since the first attempt, it showed no activity when tested. Additionally, although it measured at 1.5mg/ml by NanoDrop spectrophotometry (adjusted for a predicted extinction coefficient of 1.8), when 1µg was loaded on SDS-PAGE alongside 1µg of the original purification, the new batch gave a much weaker band.

The first purification was tested for activity, using either 1µg of the anion exchange (Q) flow through or elution, and 500ng PARP-1 as a control. In Figure 5A, PARP-1 is observed to PARylate as in the ARH3 assay, with a disappearance on the coomassie stain and a smear on the autoradiograph. By contrast, when PARP-12^{cat} anion elution was mixed with ^{32}P NAD^{+}, the coomassie band did not disappear and the autoradiograph showed a discrete band directly on top of the coomassie band. This is consistent with mono(ADP-ribosyl)ation, showed previously with PARP-10^{cat} (Kleine et al, 2008). This activity was not observed with protein collected from the anion exchange flow through. The smaller band that purified along with the PARP-12^{cat} elution also exhibited an autoradiograph signal. The flow though fraction was not tested further. When the assay was repeated with 5 minute time points (Fig. 5B), the radioactivity signal increased at each time point up to 25 minutes. The 30 minute reaction looked weaker than 25 minutes, but that may be due to a discrepancy in the amount of protein loaded in that condition.

Discussion

The first purification attempt for PARP-12^{cat} appeared easy to improve upon, but after several rounds of optimization which failed to produce active enzyme, the changes were reversed in the hope of re-creating the initial results. The final purification appeared to work until it was assayed for activity. The only step from the original purification which was not repeated was the ammonium sulfate precipitation. This step may have altered the protein in such a way as to activate it, perhaps by rearranging due to increased hydrophobic interactions. Another unusual result is the discrepancy between the first and final purifications in regards to their measured concentration. When 1μg of each was incubated with ^{32}P NAD^{+}, then analyzed by SDS-PAGE and autoradiography, the later purification appeared much weaker by coomassie staining. This might be accounted for by the ammonium sulfate precipitation, which would have removed free nucleotides from the first purification, making the OD_{280} measurement more accurate of protein content. Considering that the fourth and fifth (final) purifications were able to yield a protein of 25kDa which appeared by western blot against the 6xHis tag (in the fourth attempt), the fact they showed no activity is unexpected. The final purification should be tested again with a larger amount of protein to verify that it is not active. Perhaps its concentration, measured by NanoDrop, was not accurate and therefor gave a signal too weak to observe by autoradiography. The inability to produce more active PARP-12^{cat} hindered later attempts to test the ability of PARP-12^{cat} to mono(ADP-ribosyl)ate Ago2.

3.3 PARP-5a expression and activity

Numerous attempts to purify PARP-5a from insect cells resulted in miniscule amounts of protein overwhelmed by contaminants. The elution from nickel-affinity

chromatography did not enrich for a protein of the expected size, 142kDa. Upon western blotting with an anti-PARP-5a antibody, a signal was visible, indicating it was expressed. Anion exchange and size exclusion chromatography were unable to improve purity because of such poor results from the affinity capture. Several resins, an imidazole elution gradient and cobalt instead of nickel were tested with no improvement. After six attempts over several months, expression was abandoned to focus on re-creating a fresh bacmid, a step often suggested in troubleshooting guides. Unfortunately, ligating PARP-5a into pFastBac1, a pre-bacmid transfer vector failed despite repeated attempts.

Despite the impurity of the nickel affinity elutions, they were tested for activity, as described above for PARP-1. No activity was observed (not shown).

Discussion

Several factors may have contributed to the failure to express and purify active PARP-5a. The low expression levels may have been due to the old age of the virus provided from collaborator labs. Several insect cell protocol manuals recommended working with bacmid no more than a few months old. The efforts to create a new bacmid would have addressed this and also given the opportunity to add a second affinity tag. On the purification side, the abundance of nonspecific binding to nickel and cobalt affinity resins blocked progress beyond that first step. The only available resin that was not tested was the HiTrap Chelating HP, which improved specificity in the PARP-12^{cat} purification.

3.4 Argonaute2 ADP-ribosylation

PARP-12^{cat}, when mixed with Ago2, favored automodification activity over modification of Ago2 (Fig. 6). The Ago2 attachment control condition included radiolabeled NAD^+ to ensure that the autoradiograph signal corresponding to Ago2 in the experimental conditions could not be attributed to spontaneous chemical modification. Modification of Ago2 appeared in each experimental condition when mixed with PARP-12^{cat} except one, when the molar ratio of Ago2 to PARP-12^{cat} was 4:1. This was the only condition in which the amount of Ago2 was greater than PARP-12^{cat}. In all other conditions, a radioactivity signal corresponded with Ago2, with no apparent smearing, suggesting mono(ADP-ribosyl)ation. The signal is strongest when Ago2 was overwhelmed by PARP-12^{cat} at ratios of 1:4 and 1:8. There is a discrepancy between the two 1:4 conditions which cannot be accounted for. No signal corresponding to Ago2 or PARP-12^{cat} is visible in the only condition in which Ago2 overwhelms PARP-12^{cat}, at a ratio of 4:1. This may be due to error, as no PARP-12^{cat} automodification is visible, or because the amount of PARP-12^{cat} is too low at 62.5ng.

PARP-5a (purchased from Trevigen) showed minimal PARylation activity toward Ago2 when mixed *in vitro*. In Figure 7A, as NAD^+ concentration is decreased, the radioactivity signal corresponding to TRF1 increases. With Ago2, as NAD^+ decreases, a band corresponding to Ago2 becomes faintly visible on the autoradiograph. In both conditions, the activity of PARP-5a is primarily automodification, giving a much stronger signal than that of either substrate. With 0.3μM NAD^+, the TRF1 autoradiograph signal smears upward slightly, but this is not apparent with Ago2. When 293F cell lysate overexpressing GFP was added to the PARP-5a/Ago2 reaction, a substrate protein of approximately 120kDa appeared and the PARP-5a automodification signal decreased.

When 293F cell lysate overexpressing GFP-PARP13.2 was added, the 120kDa substrate appearance and automodification decrease were accompanied by a smear of radioactive signal both above and below 120kDa, including an enriched band corresponding to Ago2 (Fig. 7B). Adding 293T cell total RNA did not significantly change the profile of PARP-5a with Ago2, except to decrease smearing somewhat. A control with PARP-5a and BSA appeared similar to PARP-5a with Ago2, with primarily automodification activity observed.

Discussion

PARP-12^{cat} appears to be able to mono(ADP-ribosyl)ate Ago2 *in vitro* (Fig. 6). The reaction strongly favored automodification in this test. This may be due to the concentrations of each protein in this particular reaction and should be verified. There was only one condition in which the concentration of Ago2 was greater than PARP-12^{cat}, but since this condition failed to give any radiography signal, it is impossible to draw any conclusions as to whether the molar ratios of each protein contributed to the results. Two conditions had the same protein ratio but showed noticeably different signals. The purpose of this experiment was not necessarily to determine the kinetics of this interaction, but to optimize a protocol for mono(ADP-ribosyl)ation of Ago2. To achieve this, more replicates are needed and should include more conditions in which the concentration of Ago2 is greater than PARP-12^{cat}, to determine whether the reaction can be shifted away from automodification. Unfortunately, limited amounts of active PARP-12^{cat} hindered that goal.

As with PARP-12^{cat}, PARP-5a favors automodification in the assay shown in Figure 7A. Its PARylation activity toward substrate TRF1 is more robust than toward Ago2 when they are mixed in the absence of other proteins *in vitro*. Although the autoradiography signal corresponding to TRF1 increases as overall NAD^+ concentration decreases, the concentration of radiolabeled NAD^+ remains the same. There are two possible explanations for this. The lower concentration of NAD^+ could be pushing PARP-5a to favor modification of TRF1 over automodification. More likely, when the available NAD^+ is entirely radioactive, as in the lowest concentration, PAR chains attached to TRF1 are more visible by autoradiography. An autoradiography signal corresponding to Ago2 is visible at all concentrations of NAD^+ which is not present with PARP-5a alone, though this band is faint. The results seen in Figure 7B suggest that PARP-5a automodification is enhanced by the addition of other protein. PARP-5a is not visible in the coomassie stain, but can be seen at its expected size of 142kDa in the autoradiograph. The signal is faint when PARP-5a is alone, but is stronger when Ago2, 293F cell lysate or BSA is present. 293F cell lysate appears to push PARP-5a toward favoring an unknown substrate of approximately 120kDa. The appearance of additional signal above and below this size when PARP-13.2 is overexpressed suggests it is enhancing PARP-5a activity, perhaps toward all available substrates in a broad fashion. This could be the case in stress granules, where PARP-13.2, PARP-5a and Ago2 colocalize. Because PARP-5a has an RNA-binding domain, 293T cell total RNA was added to test whether it would increase PARP-5a activity toward Ago2, but that hypothesis was not supported here.

3.5 Argonaute2 cleavage activity

When incubated with its target, Ago2 loaded with endogenous insect cell RNA did not show visible cleavage activity by autoradiograph (not shown). Ago2 free of endogenous insect cell miRNA showed activity against its target when it was loaded with bantam miRNA, but not against a mutated target RNA. In the assay shown in Figure 8, the cleavage product of the bantam target is visible in lane number 4, where the target of bantam, labeled wild-type, is mixed with Ago2/bantam in a 1:5 molar ratio. While the full-length bantam target, at 40 nucleotides, makes up the majority of radiolabeled RNA visible in this condition, the cleavage product, predicted to be approximately 20 nucleotides long, is enriched compared to the control lacking Ago2. In the control, several bands appear below the full length oligonucleotide, including one at the same height as the 20bp signal from the ladder. The experimental condition has this band as well, but is enriched for an oligonucleotide just above it such that the bands overlap somewhat. Unexpectedly, the condition in which the target was mixed with Ago2/bantam in a 1:1 molar ratio gave no radioactive signal at all, likely due to error. The last three lanes, with mutant bantam target, target with Ago2/bantam in a 1:1 ratio and a 1:5 ratio, respectively, are free cleavage of products, as expected.

Discussion

Ago2 with endogenous insect cell RNA was predicted to cleave the bantam target, because bantam miRNA is present in insect cells. The lack of observed activity may have been due to a very small fraction of Ago2 carrying bantam, so little that it could not cleave enough target to be visible by autoradiography. Once bantam miRNA was

received, optimizing this reaction was not a priority. In the assay shown in Figure 8, target cleavage was achieved with pure Ago2 loaded with bantam. In an intermediate assay, both pure Ago2 and Ago2 with endogenous insect cell RNA were incubated with bantam. Presumably, bantam would have displaced some endogenous RNA from the preloaded Ago2. Results from this test were inconclusive because the reaction was loaded directly on to the denaturing urea gel without RNA extraction and much of the radioactivity signal remained in the well. To move ahead more quickly, RNA-free Ago2 was loaded with bantam for the cleavage assay shown in Figure 8. This assay is the first in which Ago2's slicer activity is observed, but only in the condition with a 1:5 ratio between target:Ago2/bantam. The absence of signal in the 1:1 ratio condition (lane 3) may be a result of error due to the numerous steps in the RNA extraction procedure, described in section 2.2.4. In the condition where cleavage appears successful, full length bantam is still the major species. These two results, the error and the low activity, should be optimized so that any possible effect of ADP-ribosylation on Ago2 will be clear.

Chapter 4

Future Directions

4.1 ARH3 activity

There are two results, discussed in section 3.1 and Figure 4, which raise interesting questions. First, when PARylated PARP-1 was treated with 5µg ARH3, the autoradiograph profile of the cleaved products was slightly different than when PARP-1 was treated with $PARG^{cat}$. It is possible that 5µg of ARH3 was not quite enough to achieve the same result, but it is also possible that the product it is leaving behind on the PARP-1 substrate are not the same terminal ADP-ribose moieties as $PARG^{cat}$. Second, when PARP-1 was treated with 50µg ARH3, the autoradiograph signal disappeared completely. This could be explained several ways. ARH3 might have removed the terminal ADP-ribose attached to PARP-1, it may have cleaved the terminal ADP-ribose between the ribose and the phosphate groups, leaving a ribose moiety on the substrate or it could be that the radioactivity signal was too weak to scan. Both this and the previous result could be resolved with thin-layer chromatography (Kleine et al, 2008), in which any remaining ADP-ribose residues or chains were separated from PARP-1 and separated by size. ARH3 should also be tested for activity against linear PAR chains built by PARP-5a as opposed to the branched PAR chains built by PARP-1.

4.2 PARP-5a expression

Difficulty in cloning PARP-5a into an insect cell expression vector stopped progress in that direction, but side-by-side cloning of the same gene into a human cell

expression vector succeeded. Because of the lab's access to and expertise with human cell cultures, this would likely be the best next step to obtain PARP-5a.

4.3 Argonaute2 ADP-ribosylation

If additional active PARP-12^{cat} can be purified, it will allow the ability to test whether mono(ADP-ribosyl)ation has an effect on the cleavage activity of Ago2. Although PARP-5a does not appear able to PARylate Ago2 alone, results discussed in section 3.5 suggest that addition of PARP-13.2 could catalyze the reaction. Achieving this with PARP-13.2 in cell lysate is messy. Using purified PARP-13.2 would be ideal. Once Ago2 is subjected to modification, it would be optimal to enrich for PARylated Ago2. One way to do this would be to use biotinylated NAD^+ so that the PAR chains could be captured by streptavidin attached to magnetic or agarose beads. These optimizations, along with those discussed in sections 3.4 and 3.5, should set up an assay that will clearly demonstrate whether mono or poly(ADP-ribosyl)ation modifies Ago2 activity *in vitro*. If modification can be shown, it should be followed by PAR digestion with PARG^{cat} and ARH3 to see whether the modification can be reversed.

Figures

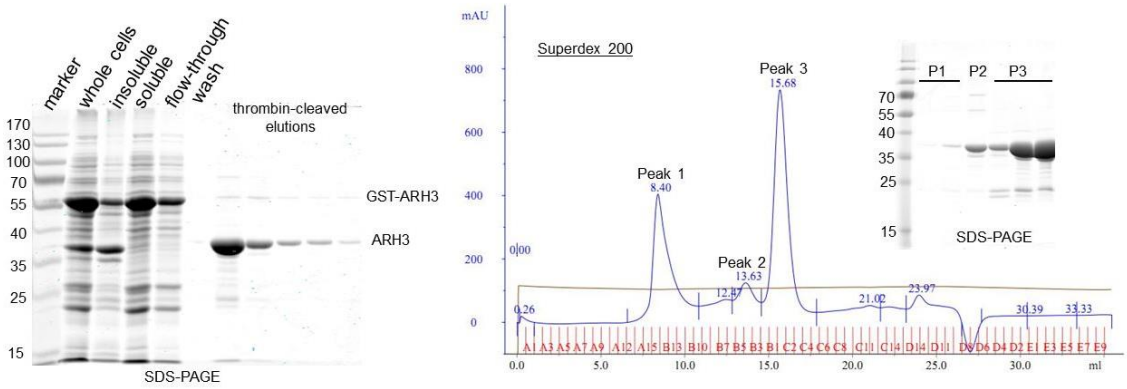

Figure 2: ARH3 purification
GST-ARH3 was expressed in *E. coli*, lysed and clarified. The soluble fraction was incubated with glutathione agarose beads. The SDS-PAGE scan on the left shows the first several steps of the purification: The beads were collected in an open gravity column, allowing unbound protein to flow through, then washed with lysis buffer. Thrombin was added to the bead slurry and incubated for 4 hours. Lysis buffer was used to washout ARH3 cleaved from the GST tag (labeled as elutions) in 5x1mL steps. These elutions were pooled, concentrated to 500µL and loaded on to an S200 size exclusion column controlled by an Äkta FPLC system. On the right is the S200 chromatogram, labeled in elution volume on the x-axis and absorbance units (at 280nm) on the y-axis. Fractions corresponding to three peaks were analyzed by SDS-PAGE, shown in an inset over the chromatogram. According to the column manufacturer, elution at 15mL corresponds to a protein of 35kDa. Peak 3 eluted at 15.68mL, indicating a protein slightly larger than 35kDa, as expected for ARH3which is 39kDa. Fractions from peak 3 were pooled, concentrated and snap-frozen for long term storage.

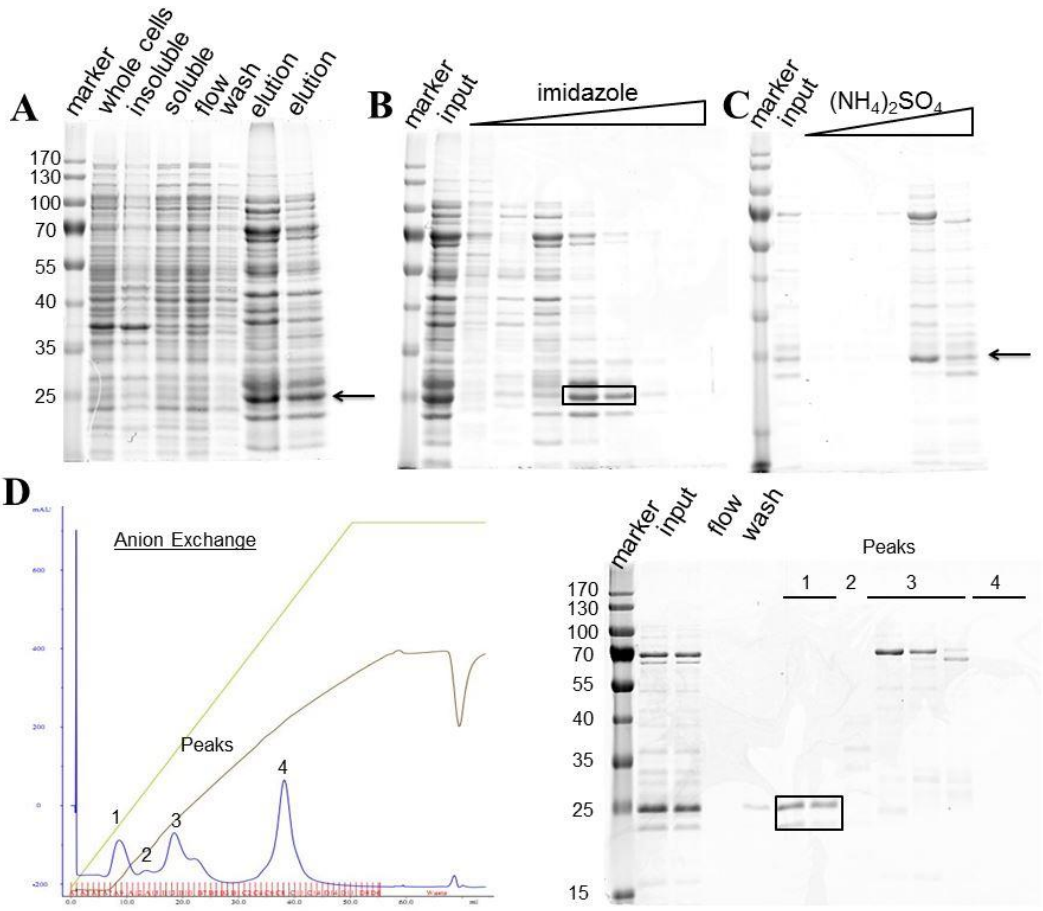

Figure 3: PARP-12^{cat} purification

PARP-12^{cat} was expressed in *E. coli* as a 6xHis fusion protein, lysed and clarified.

A. PARP-12^{cat} was captured from the soluble fraction by nickel metal affinity chromatography. An enriched band is observed, indicated with an arrow, upon elution from the nickel column with 300mM imidazole.

B. Due to the impurity of the first affinity capture, the elutions were pooled, dialyzed out of imidazole, reloaded onto the column and eluted with an imidazole step gradient. PARP-12^{cat} eluted primarily at concentrations of 100mM and 150mM imidazole, indicated inside the box. These fractions were pooled.

C. Proteins were precipitated from the previous elution by incremental addition of ammonium sulfate. Nearly all protein, including contaminants seen above and below PARP-12^{cat}, precipitated together at 40% and 50% ammonium sulfate, the two rightmost lanes. These fractions were resuspended and pooled.

D. Pooled protein was manually loaded onto an anion exchange column. The column flow-through and wash were collected. Protein was eluted from the column with a salt gradient by FPLC. PARP-12^{cat} was observed in the wash and peak 1, but only the species in peak 1 showed activity when tested (see Fig. 4). The fractions indicated by the box were pooled, concentrated and snap-frozen for long term storage.

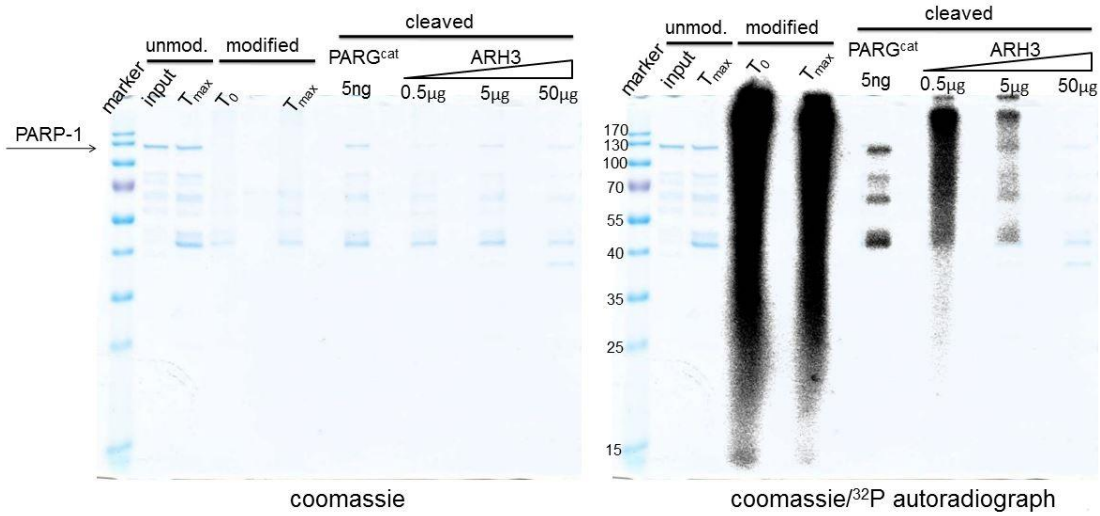

Figure 4: Purified ARH3 is an active glycohydrolase
PARP-1 was attached to magnetic nickel beads and allowed to auto-PARylate, activated by the presence of blunt-end double-stranded DNA. PAR chains were then digested with PARG or ARH3. Each reaction was run on SDS-PAGE, coomassie stained (left), then exposed to autoradiography (right, overlaid on coomassie). Input is 500ng PARP-1, followed by a bead-attachment control (T_{max}, carried through each experimental step). PARylation is visualized using ^{32}P-labeled ADP-ribose precursor NAD^+ and appears as a smear on the autoradiograph due to variable-length PAR. Modification is also observed as a disappearance of PARP-1 in the coomassie stain. This is shown in T_0 immediately after modification, and in the T_{max} control, carried through further PAR digestion steps. When PARP-1 is treated with 5ng $PARG^{cat}$, the PAR chain is digested, leaving only mono(ADP-ribose), visible as discrete bands on PARP-1 and its fragments in the autoradiograph. Treatment with ARH3 shows moderate PAR digestion at 0.5µg. With 5µg ARH3, discrete bands are evident, although the pattern is different than those in the PARG condition. With 50µg ARH3, the autoradiograph signal is totally ablated. In the coomassie stain, PARP-1 is once again visible after treatment with both $PARG^{cat}$ and ARH3. This indicates the variable-length PAR chains are gone. In the rightmost lane, a band the size of ARH3 appears in the coomassie stain. Because the concentration of ARH3 was so high in this condition, some may have nonspecifically bound to the magnetic beads and not completely washed away.

A

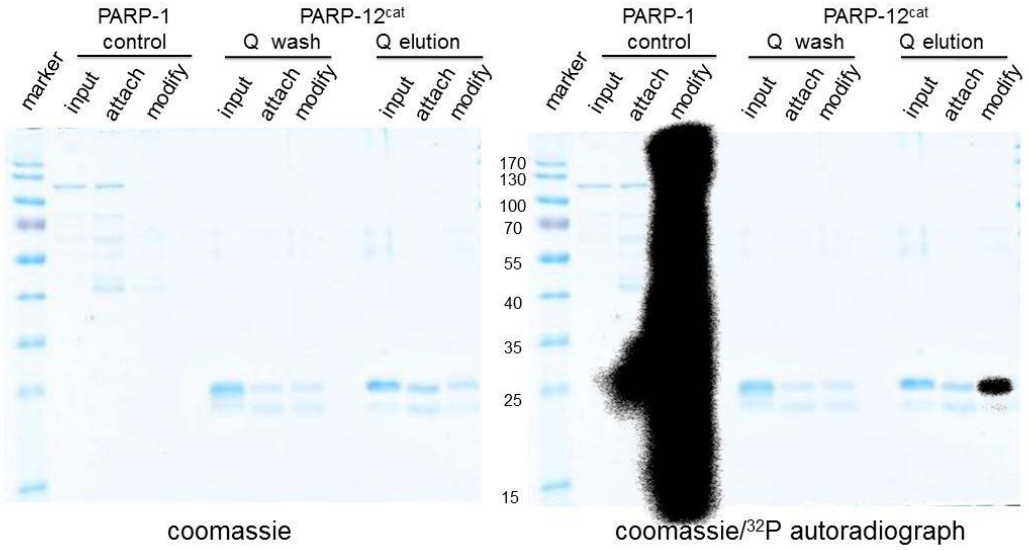

B

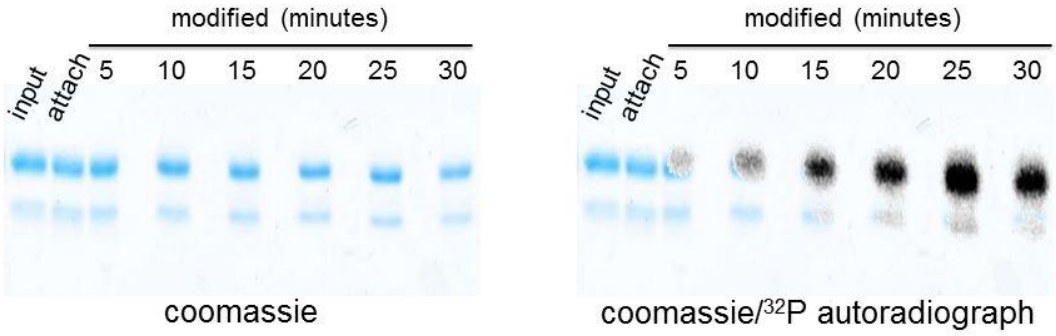

Figure 5: Purified PARP-12^{cat} is an active mono(ADP-ribose) transferase
A. PARP-12 catalytic domain was attached to magnetic nickel beads and allowed to automodify in the presence of ^{32}P-labeled NAD^{+}. PARP-1 is included for comparison. Two populations of PARP-12^{cat} were tested for activity: one of which eluted from HiTrap Q anion exchange during the wash step, and another which eluted at a low NaCl concentration (elution). Reactions were run on SDS-PAGE, coomassie stained (left) then exposed to autoradiography (right, overlaid on coomassie). Included is a loading control of 500ng for PARP-1 and 1µg for each PARP-12^{cat} species. Also included is an attachment lane to control for the amount of protein affixed to the beads. PARylation of PARP-1 is observed by a disappearance in the modification lane on the coomassie stain and a smear on the autoradiograph. In contrast, no disappearance is visible with PARP-12^{cat} modification, but a discrete band is visible upon autoradiography. The presence of a radioactive signal, but lack of mobility shift, is characteristic of mono(ADP-ribosyl)ation.
B. As the reaction progresses, the radioactivity signal becomes stronger, saturating at 25 minutes.

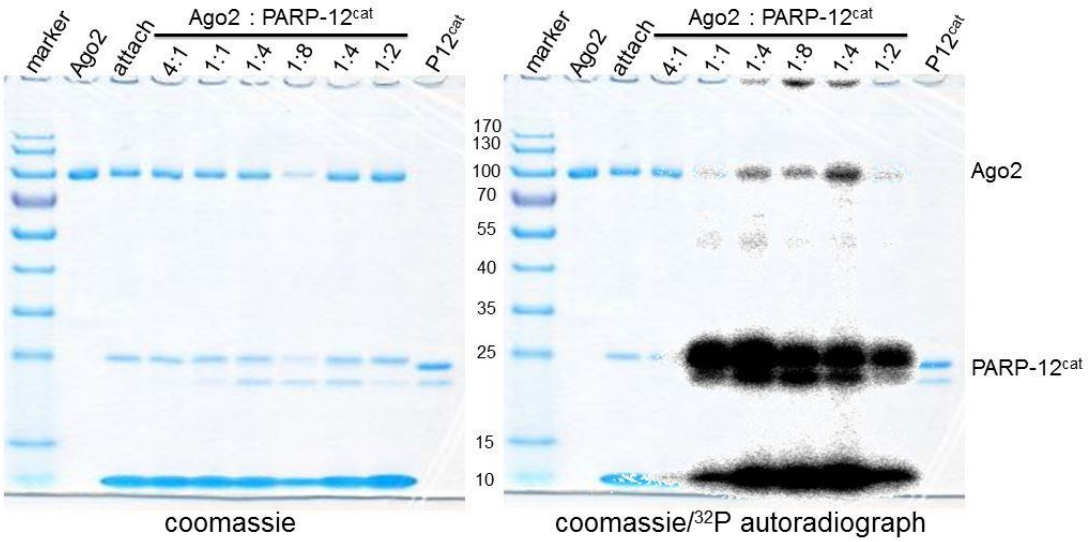

Figure 6: Ago2 mono(ADP-ribosyl)ation by PARP-12^{cat}

Ago2 was attached to MagStrep beads and mixed with PARP-12^{cat} in various molar ratios, and with ^{32}P-lableled NAD^{+}. The experimental conditions above lie under the horizontal line. In the first three conditions, Ago2 is constant at 1µg while the amount of PARP-12^{cat} is varied. In the next three conditions, PARP-12^{cat} is constant at 1µg while the amount of Ago2 is varied. In addition to the experimental conditions, radiolabeled NAD^{+} is included in the attachment control. The ADP-ribosylation activity of PARP-12^{cat} favors automodification, but modification of Ago2 is visible.

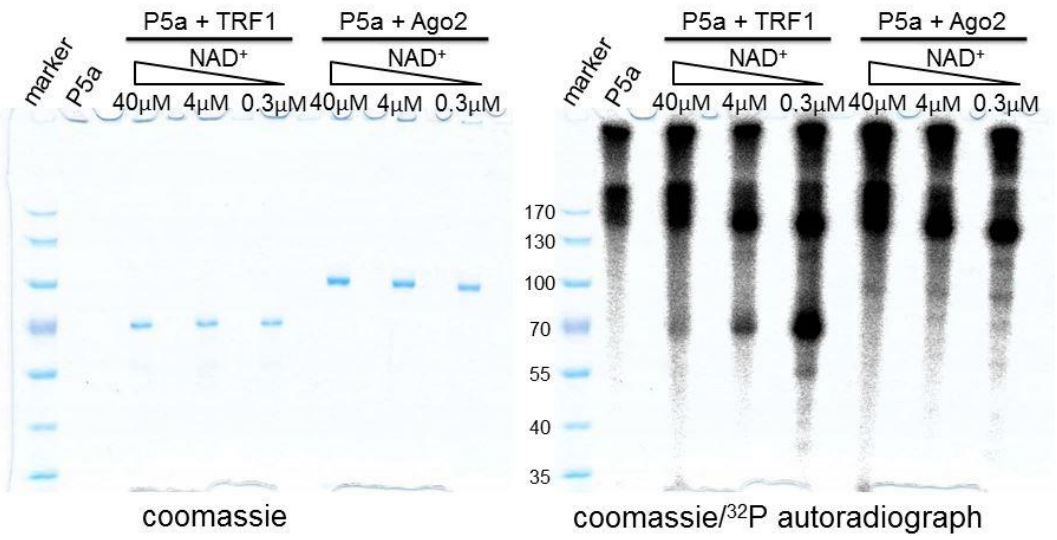

Figure 7A: Ago2 poly(ADP-ribosyl)ation by PARP-5a
TRF1 was attached to magnetic nickel beads; Ago2 was attached to MagStrep beads. Both were mixed with PARP-5a and various concentrations of NAD^+. The overall concentration of non-radioactive NAD^+ was varied, but the amount that was ^{32}P-labeled was always 0.3μM. A band corresponding to TRF1 increases in strength on the autoradiograph as the concentration of NAD^+ decreases, while only a faint band corresponding to Ago2 is visible at all concentrations.

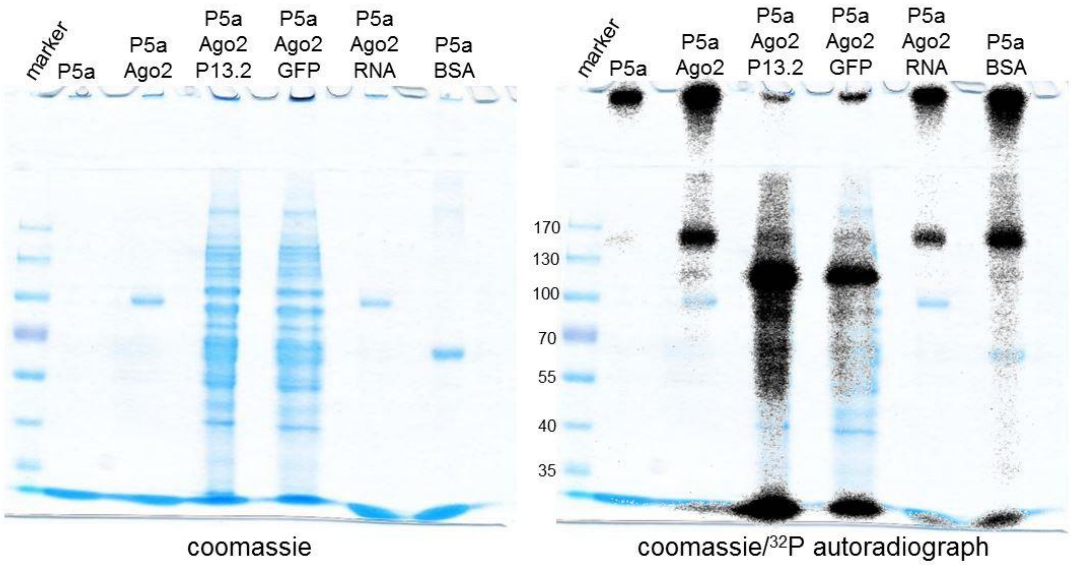

Figure 7B: Ago2 poly(ADP-ribosyl)ation by PARP-5a

Ago2 was attached to MagStrep beads and mixed with PARP-5a alone or with one of several additions: lysate from 293F cells overexpressing GFP-PARP-13.2 or GFP only or total RNA from 293T cells. BSA was also tested with PARP-5a as a non-specific substrate. Compared with PARP-5a alone, all additives increased automodification activity. No autoradiograph signal corresponds to Ago2 or BSA when they were mixed with PARP-5a only. A signal may be visible corresponding to Ago2 when PARP-13.2 lysate is added, but it is overwhelmed by a smear, including a strong band around 120kDa.

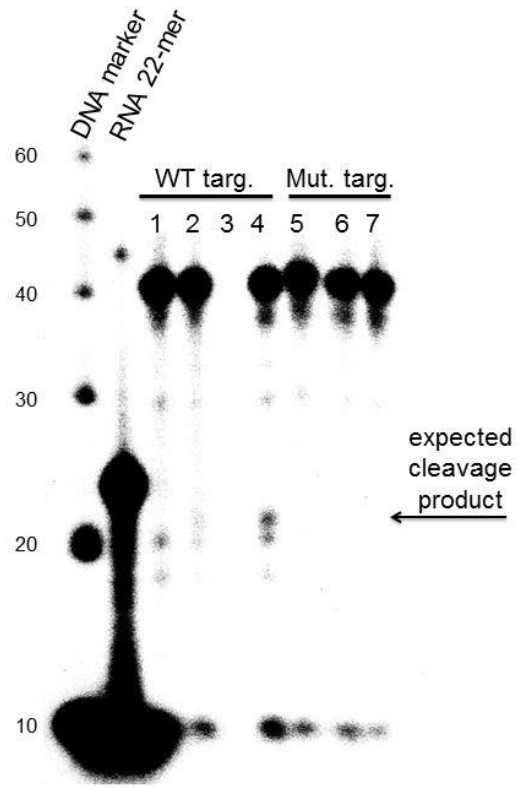

Figure 8: Ago2-mediated RNA cleavage assay
Wild-type bantam target RNA or a mutated target were 5' ^{32}P-phospholabeled. RNA-free Ago2 was loaded with bantam miRNA and mixed with the bantam target or the mutant target in two molar ratios. An RNase inhibitor, SUPERase In was used to prevent nonspecific cleavage in all conditions except (2), where a different inhibitor, RNase OUT, was tested. RNA from each reaction was isolated from protein and electrophoresed on a denaturing urea gel which was then exposed overnight to autoradiography for analysis. A 10-base pair DNA marker and an RNA 22-mer, both radiolabeled, were also run for size comparison. Reactions, from left to right: (1) WT target, (2) WT target:Ago2/bantam 1:1 with RNase OUT, (3) WT target:Ago2/bantam 1:1, (4) WT target:Ago2/bantam 1:5, (5) Mut. target, (6) Mut. target:Ago2/bantam 1:1, (7) Mut. target:Ago2/bantam 1:5. The expected size of the bantam target cleavage product is 20 nucleotides. A band between the 20 base pair DNA marker and the RNA 22-mer appears in conditions 2 and 4, which is not visible in the control, 1. The lack of any signal in condition 3 is likely the result of error. As expected, this cleavage product is not visible in any of the conditions when the target is mutated.

References

Atasheva S, Akhrymuk M, Frolova EI, Frolov I (2012) New PARP Gene with an Anti-Alphavirus Function. *Journal of Virology* **86:** 8147-8160

Bürkle A (2005) Poly(ADP-ribose). The most elaborate metabolite of NAD+. *FEBS Journal* **272:** 4576-4589

Feijs KLH, Verheugd P, Lüscher B (2013) Expanding functions of intracellular resident mono-ADP-ribosylation in cell physiology. *FEBS Journal* **280:** 3519-3529

Gibson BA, Kraus WL (2012) New insights into the molecular and cellular functions of poly(ADP-ribose) and PARPs. *Nature Reviews Molecular Cell Biology* **13:** 411-424

Griffiths-Jones S, Grocock RJ, van Dongen S, Bateman A, Enright AJ (2006) miRBase: microRNA sequences, targets and gene nomenclature. *Nucleic Acids Research* **34:** D140-D144

Guettler S, LaRose J, Petsalaki E, Gish G, Scotter A, Pawson T, Rottapel R, Sicheri F (2011) Structural Basis and Sequence Rules for Substrate Recognition by Tankyrase Explain the Basis for Cherubism Disease. *Cell* **147:** 1340-1354

Guo H, Ingolia NT, Weissman JS, Bartel DP (2010) Mammalian microRNAs predominantly act to decrease target mRNA levels. *Nature* **466:** 835-840

Hayakawa S, Shiratori S, Yamato H, Kameyama T, Kitatsuji C, Kashigi F, Goto S, Kameoka S, Fujikura D, Yamada T, Mizutani T, Kazumata M, Sato M, Tanaka J, Asaka M, Ohba Y, Miyazaki T, Imamura M, Takaoka A (2010) ZAPS is a potent stimulator of signaling mediated by the RNA helicase RIG-I during antiviral responses. *Nature Immunology* **12:** 37-44

Hsiao SJ, Smith S (2008) Tankyrase function at telomeres, spindle poles, and beyond. *Biochimie* **90:** 83-92

Jankevicius G, Hassler M, Golia B, Rybin V, Zacharias M, Timinszky G, Ladurner AG (2013) A family of macrodomain proteins reverses cellular mono-ADP-ribosylation. *Nature Structural & Molecular Biology* **20:** 508-514

Kerns JA, Emerman M, Malik HS (2008) Positive Selection and Increased Antiviral Activity Associated with the PARP-Containing Isoform of Human Zinc-Finger Antiviral Protein. *PLoS Genetics* **4:** e21

Kernstock S, Koch-Nolte F, Mueller-Dieckmann J, Weiss MS, Mueller-Dieckmann C (2006) Cloning, expression, purification, crystallization and preliminary X-ray diffraction analysis of human ARH3, the first eukaryotic protein-ADP-ribosylhydrolase. *Acta Crystallographica Section F Structural Biology and Crystallization Communications* **62:** 224-227

Kim I-K, Kiefer JR, Ho CMW, Stegeman RA, Classen S, Tainer JA, Ellenberger T (2012) Structure of mammalian poly(ADP-ribose) glycohydrolase reveals a flexible tyrosine clasp as a substrate-binding element. *Nature Structural & Molecular Biology* **19:** 653-656

Kleine H, Poreba E, Lesniewicz K, Hassa PO, Hottiger MO, Litchfield DW, Shilton BH, Lüscher B (2008) Substrate-Assisted Catalysis by PARP10 Limits Its Activity to Mono-ADP-Ribosylation. *Molecular Cell* **32:** 57-69

Krol J, Loedige I, Filipowicz W (2010) The widespread regulation of microRNA biogenesis, function and decay. *Nature Reviews Genetics*

Lehtiö L, Collins R, van den Berg S, Johansson A, Dahlgren L-G, Hammarström M, Helleday T, Holmberg-Schiavone L, Karlberg T, Weigelt J (2008) Zinc Binding Catalytic Domain of Human Tankyrase 1. *Journal of Molecular Biology* **379:** 136-145

Leung Anthony KL, Vyas S, Rood Jennifer E, Bhutkar A, Sharp Phillip A, Chang P (2011) Poly(ADP-Ribose) Regulates Stress Responses and MicroRNA Activity in the Cytoplasm. *Molecular Cell* **42:** 489-499

Lin W, Ame J-C, Aboul-Ela N, Jacobson EL, Jacobson MK (1997) Isolation and Characterization of the cDNA Encoding Bovine

Poly(ADP-ribose) Glycohydrolase. *The Journal of Biological Chemistry* **272:** 11895-11901

Liu J, Carmell MA, Rivas FV, Marsden CG, Thompson JM, Song J-J, Hammond SM, Joshua-Tor L, Hannon GJ (2004) Argonaute2 Is the Catalytic Engine of Mammalian RNAi. *Science* **305:** 1437-1441

Luo X, Kraus WL (2012) On PAR with PARP: cellular stress signaling through poly(ADP-ribose) and PARP-1. *Genes & Development* **26:** 417-432

Meister G, Landthaler M, Patkaniowska A, Dorsett Y, Teng G, Tuschl T (2004) Human Argonaute2 Mediates RNA Cleavage Targeted by miRNAs and siRNAs. *Molecular Cell* **15:** 185-197

Meyer-Ficca ML, Meyer RG, Coyle DL, Jacobson EL, Jacobson MK (2004) Human poly(ADP-ribose) glycohydrolase is expressed in alternative splice variants yielding isoforms that localize to different cell compartments. *Experimental Cell Research* **297:** 521-532

Meyer RG, Meyer-Ficca ML, Whatcott CJ, Jacobson EL, Jacobson MK (2007) Two small enzyme isoforms mediate mammalian mitochondrial poly(ADP-ribose) glycohydrolase (PARG) activity. *Experimental Cell Research* **313:** 2920-2936

Mueller-Dieckmann C, Kernstock S, Lisurek M, von Kries JP, Haag F, Weiss MS, Koch-Nolte F (2006) The structure of human ADP-ribosylhydrolase 3 (ARH3) provides insights into the reversibility of protein ADP-ribosylation. *Proceedings of the National Academy of Sciences* **103:** 15026-15031

Niere M, Mashimo M, Agledal L, Dolle C, Kasamatsu A, Kato J, Moss J, Ziegler M (2012) ADP-ribosylhydrolase 3 (ARH3), Not Poly(ADP-ribose) Glycohydrolase (PARG) Isoforms, Is Responsible for Degradation of Mitochondrial Matrix-associated Poly(ADP-ribose). *Journal of Biological Chemistry* **287:** 16088-16102

Oka S, Kato J, Moss J (2005) Identification and Characterization of a Mammalian 39-kDa Poly(ADP-ribose) Glycohydrolase. *Journal of Biological Chemistry* **281:** 705-713

Parker JS, Roe SM, Barford D (2004) Crystal structure of a PIWI protein suggests mechanisms for siRNA recognition and slicer activity. *The EMBO Journal* **23:** 4727 - 4737

Rivas FV, Tolia NH, Song J-J, Aragon JP, Liu J, Hannon GJ, Joshua-Tor L (2005) Purified Argonaute2 and an siRNA form recombinant human RISC. *Nature Structural & Molecular Biology* **12:** 340-349

Rosenthal F, Feijs KLH, Frugier E, Bonalli M, Forst AH, Imhof R, Winkler HC, Fischer D, Caflisch A, Hassa PO, Lüscher B, Hottiger MO (2013) Macrodomain-containing proteins are new mono-ADP-ribosylhydrolases. *Nature Structural & Molecular Biology* **20:** 502-507

Sharifi R, Morra R, Denise Appel C, Tallis M, Chioza B, Jankevicius G, Simpson MA, Matic I, Ozkan E, Golia B, Schellenberg MJ, Weston R, Williams JG, Rossi MN, Galehdari H, Krahn J, Wan A, Trembath RC, Crosby AH, Ahel D, Hay R, Ladurner AG, Timinszky G, Williams RS, Ahel I (2013) Deficiency of terminal ADP-ribose protein glycohydrolase TARG1/C6orf130 in neurodegenerative disease. *The EMBO Journal* **32:** 1225-1237

Slade D, Dunstan MS, Barkauskaite E, Weston R, Lafite P, Dixon N, Ahel M, Leys D, Ahel I (2011) The structure and catalytic mechanism of a poly(ADP-ribose) glycohydrolase. *Nature* **477:** 616-620

Smith S, Giriat I, Schmitt A, de Lange T (1998) Tankyrase, a Poly(ADP-Ribose) Polymerase at Human Telomeres. *Science* **282:** 1484-1487

Vyas S, Chesarone-Cataldo M, Todorova T, Huang Y-H, Chang P (2013) A systematic analysis of the PARP protein family identifies new functions critical for cell physiology. *Nature Communications* **4:** 2240

Wee Liang M, Flores-Jasso CF, Salomon William E, Zamore Phillip D (2012) Argonaute Divides Its RNA Guide into Domains with Distinct Functions and RNA-Binding Properties. *Cell* **151:** 1055-1067

Ryan Weltzer

933 Saint Paul St., Apt. B5
Baltimore, MD 21202
517.410.2462 • ryan.weltzer@gmail.com
Date of Birth: August 6, 1982, Kalamazoo, MI

EDUCATION

Master of Science (ScM) November 2013
Johns Hopkins Bloomberg School of Public Health, Baltimore, MD
Department of Biochemistry and Molecular Biology
Thesis: In Vitro Reconstitution of Argonaute poly(ADP-ribosyl)ation and Its Impact on microRNA Activity.
Selected Coursework: Principles of Immunology I&II, Statistical Reasoning I&II, Stem Cells, Genome Integrity and Cancer, Politics of Health Policy, U.S. Healthcare

Bachelor of Arts (BA)
Michigan State University, East Lansing, MI December 2007
Concentration: Interdisciplinary Studies – International Studies
Cognate: Psychology
Specialization: Bioethics, Humanities and Society

RESEARCH EXPERIENCE

Laboratory Technician 2009-2012
Johns Hopkins Bloomberg School of Public Heath, Baltimore, MD
Bosch Lab, Department of Biochemistry and Molecular Biology/Malaria Research Institute
•Protein purification to identify anti-malarial drug targets
•Publication: Hain, A.U.P., **Weltzer, R.R.**, et. al. Structural characterization and inhibition of the Plasmodium Atg8-Atg3 interaction (2012) *Journal of Structural Biology*, 180 (3), pp. 551-562.

NONPROFIT/TEACHING EXPERIENCE

Youth Development Counselor 2008-2010
Children's Beach House, Lewes, DE
Advocacy Coordinator, Trainer, Sexual Assault Counselor 2005-2008
The Listening Ear Crisis Center, East Lansing, MI
Substitute Teacher 2006-2008
Ingham Intermediate School District, Mason, MI

PROFESSIONAL DEVELOPMENT

Computer Skills: Microsoft Office **Languages:** Spanish (conversational) **Certifications:** Emergency Medical Technician – Basic **Other teaching/training:** Karate instructor (2010-present) **Volunteer:** Diane Byrum for Congress (2000), Habitat for Humanity (2005)